Available online at www.sciencedirect.com
ScienceDirect
Journal of Sound and Vibration 304 (2007) 793–810
JOURNAL OF SOUND AND VIBRATION
www.elsevier.com/locate/jsvi

Acoustic tuning of gas–liquid scheme injectors for acoustic damping in a combustion chamber of a liquid rocket engine

Chae Hoon Sohn[a,*], I-Sun Park[a], Seong-Ku Kim[b], Hong Jip Kim[b]

[a]*Department of Mechanical Engineering, Sejong University, Seoul 143-747, Republic of Korea*
[b]*Korea Aerospace Research Institute, Daejeon 305-333, Republic of Korea*

Received 1 August 2005; received in revised form 1 June 2006; accepted 17 March 2007

Abstract

In a combustion chamber of a liquid rocket engine, acoustic fine-tuning of gas–liquid scheme injectors is studied numerically for acoustic stability by adopting a linear acoustic analysis. Injector length and blockage ratio at gas inlet are adjusted for fine-tuning. First, acoustic behavior in the combustor with a single injector is investigated and acoustic-damping effect of the injector is evaluated for cold condition by the quantitative parameter of damping factor as a function of injector length. From the numerical results, it is found that the injector can play a significant role in acoustic damping when it is tuned finely. The optimum tuning-length of the injector to maximize the damping capacity corresponds to half of a full wavelength of the first longitudinal overtone mode traveling in the injector with the acoustic frequency intended for damping in the chamber. In baffled chamber, the optimum lengths of the injector are calculated as a function of baffle length for both cold and hot conditions. Next, in the combustor with numerous resonators, peculiar acoustic coupling between a combustion chamber and injectors is observed. As the injector length approaches a half-wavelength, the new injector-coupled acoustic mode shows up and thereby, the acoustic-damping effect of the tuned injectors is appreciably degraded. And, damping factor maintains a near-constant value with blockage ratio and then, decreases rapidly. Blockage ratio affects also acoustic damping and should be considered for acoustic tuning.

1. Introduction

Acoustic instability is a phenomenon in which pressure oscillations are amplified through in-phase thermal interaction with combustion [1,2]. This may result in an intense pressure fluctuation as well as excessive heat transfer to combustor walls in systems such as solid and liquid propellant rocket engines, ramjets, turbojet thrust augmentors, utility boilers, and furnaces [3]. Accordingly, it has gained significant interest in propulsion and power systems. Although it has caused common problems in these systems, it has been reported that it occurs most severely in liquid rocket engines due to their high-energy density. Thermal damage on injector faceplate and combustor wall, severe mechanical vibration of rocket body, and unpredictable malfunction of engines, etc. are usual problems caused by acoustic instability. To understand this phenomenon, lots of studies have been conducted [1,4–8], but it is still being pursued.

*Corresponding author.
E-mail address: chsohn@sejong.ac.kr (C.H. Sohn).

0022-460X/$ - see front matter © 2007 Elsevier Ltd. All rights reserved.
doi:10.1016/j.jsv.2007.03.036

Nomenclature

B	blockage ratio at gas propellant (injector) inlet, defined in Eq. (9)
c	sound speed in the medium
D_{ch}	diameter of the chamber
D_{th}	diameter of nozzle throat
d_{in}	orifice diameter at gas propellant (injector) inlet
d_{inj}	inner diameter of the injector
f	frequency
f_0	tuning frequency or acoustic frequency of pressure oscillation in the chamber
k	wavenumber defined by ω/c_0
L_{th}	length from injector faceplate to nozzle throat
L_e	length from injector faceplate to nozzle entrance
L_{eff}	effective chamber length used in Eq. (8)
L^*_{inj}	effective injector length used in Eq. (8)
l	length
$\mathbf{M}$	Mach number of the mean flow
N_p	number of grid points
$\tilde{P}$	complex acoustic pressure
p'	pressure fluctuation
t	time
$\mathbf{x}$	spatial coordinate vector
x, y, z	physical coordinates
Z	acoustic impedance
Δl	length correction factor
β	boundary absorption coefficient
η	damping factor defined in Eq. (6)
λ	wavelength of longitudinal pressure oscillation within gas passage of injector
ρ	density
σ_A	open-area ratio, or the ratio of open area to faceplate area
ω	angular frequency

Subscripts

baf	baffle
inj	injector or state of the fluid in the injector
peak	peak response
R	resonator
0	state of the fluid in the chamber
$1T$	the first tangential acoustic mode
$1L$	the first longitudinal acoustic mode

Superscript

$\sim$	complex variable

There have been adopted two methods in the control of acoustic instability, classified into passive and active controls [4,9]. Passive control is to attenuate acoustic oscillation using combustion stabilization devices such as baffles, acoustic resonators, and acoustic liners. For example, acoustic resonator can damp out or absorb pressure wave oscillating in the chamber using well-tuned cavity [9–11]. Although active control is studied and tested recently as an improved control method [12,13], the most reliable method to suppress acoustic-pressure oscillation is still to install baffle or resonators on/near the injector faceplate. Through numerous studies and tests [4,5,9,10,14–16] conducted during the engine development, design criteria on baffle and acoustic resonator have been established with good confidence. However, the devices are installed additionally and inevitably to suppress undesirable acoustic oscillations if they should be. And thus, negative effects of engine-performance degradation and complexity in engine manufacture accompany the installation of these devices.

On the other hand, in liquid rocket engines, injectors are mounted necessarily to the faceplate in order to inject propellants into the chamber. Depending on the phase of the injected propellants, they are classified into liquid-liquid scheme and gas–liquid scheme injectors. In the pump-fed liquid rocket engines of high-performance, staged combustion cycle is usually employed, where preburner is used and regenerative cooling is adopted for the cooling of combustor wall [17]. In this system, the coaxial and gas–liquid scheme injector is typically used, which is illustrated in Fig. 1. As shown in this figure, gaseous oxidizer (GO_x) flows through the inner passage of the injector and then, it is mixed with liquid hydrocarbon fuel injected through several peripheral holes and finally, both GO_x and liquid fuel are injected into the chamber [18]. At this point, with the inside volume of the injector occupied by gas, it is worthy of note that the gas–liquid scheme injectors may play a significant role in acoustic damping like acoustic resonators in addition to its original function of propellants injection. If it is true of the injector, proper design of the injector shall attenuate pressure oscillation to a good degree and eventually, we can do without additional installation of baffle or resonator.

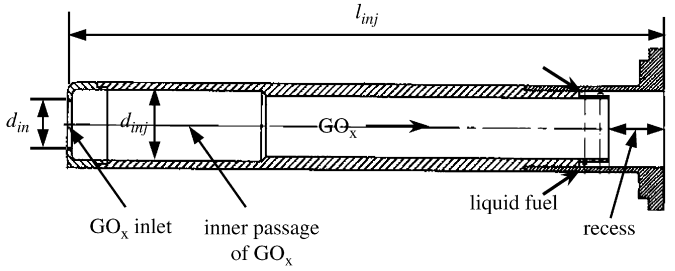

Fig. 1. Geometry of the coaxial and gas–liquid scheme injector.

In this regard, acoustic tuning of gas–liquid scheme injector is investigated intensively here. The present study provides new information concerning injector design for acoustic tuning; the possibility of acoustic damping by tuning the injector, optimum size of the injector for maximum acoustic damping, and acoustic coupling between chamber and injectors. For this, acoustic behaviors in the chambers with both a single injector and numerous injectors are investigated numerically by adopting linear acoustic analysis.

2. Numerical methods

2.1. Governing equation

Acoustic field in the chamber is calculated by solving wave equation [19]. In the present study, only acoustic behavior is studied and combustion processes are not considered. For a homogeneous and non-dissipative medium, the linear wave equation can be derived as [20,21]

$$\nabla^2 p' - \frac{1}{c_0^2}\frac{\partial^2 p'}{\partial t^2} - \frac{2}{c_0}\frac{\partial}{\partial t}(\mathbf{M}\cdot\nabla p') - (\mathbf{M}\cdot\nabla)(\mathbf{M}\cdot\nabla p') = 0, \tag{1}$$

where p' denotes pressure fluctuation, c_0 sound speed in the medium, t time, and $\mathbf{M}$ Mach number of the mean flow. At this point, all acoustic variables are assumed to be temporally periodic for a given frequency, f. With this harmonic assumption, unsteady solution in time domain can be transformed to steady solution in frequency domain, and thus, time-varying pressure fluctuation of $p'(\mathbf{x}, t)$ is expressed by complex acoustic pressure $\tilde{P}(\mathbf{x})$ in the form

$$p'(\mathbf{x}, t) = \mathrm{Re}\{\tilde{p}'(\mathbf{x}, t)\} = \mathrm{Re}\{\tilde{P}(\mathbf{x})\mathrm{e}^{-\mathrm{i}\omega t}\}, \tag{2}$$

where tilde (˜) denotes complex variable, Re the real part of complex variable, and $\omega = 2\pi f$ the angular frequency. In this study, convection of acoustic field is not considered, namely, $\mathbf{M} = 0$. With Eq. (2) and this simplification, the wave equation, Eq. (1) leads to the well-known Helmholtz equation

$$\frac{\partial^2 \tilde{P}}{\partial x^2} + \frac{\partial^2 \tilde{P}}{\partial y^2} + \frac{\partial^2 \tilde{P}}{\partial z^2} + k^2 \tilde{P} = 0, \tag{3}$$

where k denotes wavenumber defined as ω/c_0 or $2\pi f/c_0$. The harmonic analysis with Eq. (3) makes the problem much easier than solving the unsteady wave equation (Eq. (1)).

To solve Eq. (3), an in-house finite element method (FEM) code named KAA3D [21] is employed here. Eq. (3) is discretized in space by Galerkin's procedure [22] with the identical linear weighting and test functions on four-type hybrid elements (hexahedral, tetrahedral, prism, and pyramid). To deal with complex geometry, computational mesh can be generated by either an expert user-made grid generator or a commercial software (GAMBIT, Fluent corporation) with a transformation of grid connectivity to be appropriate for KAA3D code. With the number of grid points, N_p, the $N_p \times N_p$ discretized equation set consists of real and imaginary parts and is transformed to $2N_p \times 2N_p$ real system through equivalent real formulation. To enhance convergence and effectiveness for a large number of grid points (especially, N_p greater than 30,000), the resultant sparse matrix is solved using GMRES (Generalized Minimal Residual) iterative technique with ILUT (Incomplete LU factorization with dual truncation strategy) preconditioner [23].

In the previous works [21,24], the acoustic results calculated by KAA3D showed good agreement with analytic and experimental data and it has been used successfully for the design of combustion stabilization devices. More details on numerical methods and calculation procedures adopted in KAA3D can be found in the literature [21,24].

2.2. Geometric models of combustion chamber and injector

The geometry and computational grids of the chamber to be analyzed are shown in Fig. 2. Usually, the combustion chamber of liquid rocket engine has numerous injectors mounted to faceplate. Before considering all the injectors, only one injector will be first considered. The effect of multi-injectors on this first approximation will then be checked. Accordingly, the chamber with a single injector is considered first as shown in Fig. 2. The computational domain ranges from the injector faceplate to nozzle throat including injector itself. The chamber geometry has been taken from one variant of liquid rocket engines under development for future use. The diameters of the chamber and the nozzle throat, D_{ch} and D_{th}, are 380 and 190 mm, respectively. The lengths from the faceplate to nozzle entrance and the throat, L_e and L_{th}, are 250 and 478 mm, respectively, and a half-contraction angle in the conical section is 30°. Although, the inner passage of the gas–liquid scheme injector can frequently have tapered or stepped shapes as shown in Fig. 1, the straight passage is assumed here for simplicity and clarity of acoustic investigation. Besides, it is assumed that the injector has no recess for the same purpose. Accordingly, it has complete cylindrical shape with inner diameter of d_{inj}. The injector diameter dose not affect numerical results in a qualitative manner, but only damping capacity. Accordingly, it can have arbitrary value for the present research purposes. As an example, the injector diameter is selected to be 14 mm in case of single-injector mounting and enlarged into 30 mm in case of multi-injectors mounting. In this study, the injector length, l_{inj} and the blockage ratio, B are the critical parameters for acoustic tuning and thus, acoustic field is calculated with variable parameters of l_{inj} and B. The definition of blockage ratio, B can be found in later section. With widely used injectors, d_{in} is less than d_{inj} as shown in Fig. 1 and B is greater than zero (0).

The chamber wall and the faceplate have rigid-wall boundary condition. In actual reactive flows, the sonic condition is formed at the nozzle throat and thus, with negligible error, the throat can be considered to be acoustically closed end which reflects all the incident waves without loss or amplification. In other words, it acts as a rigid wall on acoustics although it has physically open condition for mean flow. Our preliminary

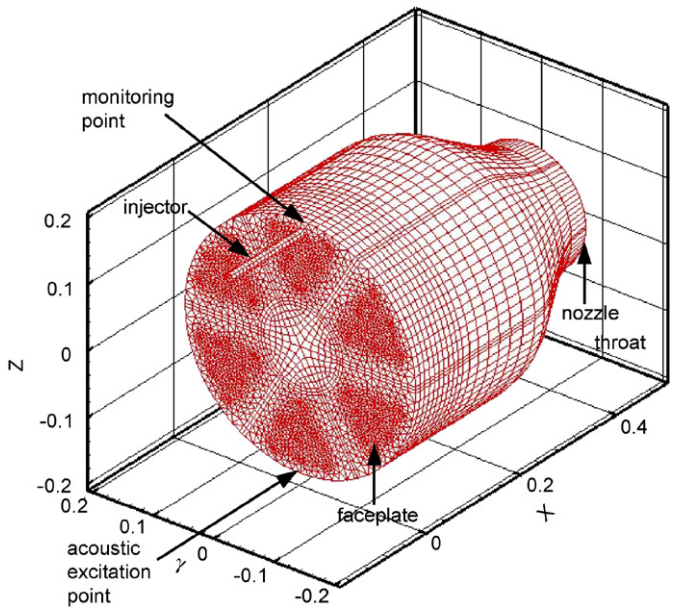

Fig. 2. Geometry and computational grids of the chamber with a single injector.

calculation with application of admittance boundary condition, taken from the literature [1], at the nozzle throat revealed that acoustic radiation from the nozzle hardly affected resonant frequencies and contributed a little to increase in damping factor, η. For this reason, the computational domain shown in Fig. 2 excludes the nozzle expansion part downstream of the throat since the part does not affect the acoustic field within the chamber. With these boundary conditions, most of acoustic analyses here are conducted for cold-volume condition. That is, the medium is assumed to be a quiescent air ($\mathbf{M} = 0$) of which density, ρ_0 and sound speed, c_0 are 1.2 kg/m^3 and 340 m/s, respectively. The assumption of quiescent medium can be justified by the fact that mean flow affects resonant frequencies of transverse acoustic modes only by the factor of $\sqrt{1-\mathbf{M}^2}$ [25]. Especially, tangential acoustic modes are little affected by the mean flow in the usual range of $\mathbf{M}$ ($=0.1\sim0.2$) in a rocket combustion chamber. When combustion processes are considered, combustion field can be simulated by adjusting the values of ρ_0 and c_0 suitable for hot condition. In a combustion chamber, spatially non-homogeneous temperature distribution is established, which may affect acoustic behavior. But, the previous work [26] showed that temperature distribution did not change fundamental aspects of acoustic behavior, but only natural frequencies through variation of sound speed, c_0. Accordingly, acoustic tuning can be investigated by adopting homogeneous temperature field, i.e., uniform sound speed in a combustion chamber. Furthermore, it has been reported that acoustic calculations for cold condition can offer good results and information in the acoustic point of view [1,9,10]. Accordingly, the present analyses are focused on cold condition and the analyses for hot condition are conducted to obtain the quantitative data.

2.3. Numerical procedures

Numerical procedures are quite similar to the acoustic experimental tests [9,10,27] as demonstrated in Fig. 2. Acoustic excitation is numerically imposed from sound source, which corresponds to loudspeaker, located on the faceplate near the chamber wall. The acoustic-pressure response is monitored by acoustic amplitude at the monitoring point, where clear response is made. The monitoring point is located on the faceplate near the chamber wall at the opposite side to the sound source. Sine-wave acoustic oscillation is generated by the sound source with arbitrary acoustic amplitude of 10 Pa and the acoustic frequency sweeping from 300 to 1000 Hz for cold condition. By doing so, we obtain the acoustic response of the fluid within the chamber as a function of the frequency of acoustic excitation.

Boundary condition at wall is set up as follows. At the rigid wall, theoretical value of acoustic impedance, Z is infinitely large and boundary absorption coefficient, β, defined by $\rho_0 c_0/Z$, becomes zero (0) [28]. This indicates that there is no boundary absorption of sound wave and thereby, acoustic amplitude becomes infinitely large at any acoustic resonant modes of the chamber. But, in the actual combustor, acoustic oscillation with infinitely large amplitude is not observed due to boundary absorption at the chamber wall. To consider this point, boundary absorption coefficient of 0.005 is used, which resulted from the experiment [21,29].

The number of computational grids is 65,000 or so in both unbaffled and baffled chambers; "unbaffled" chamber indicates the chamber without baffle installation. Through grid-dependency check of the numerical results, this grid system was found to give good accuracy.

3. Acoustic consideration of injector's role as a resonator

Acoustic resonators or absorbers have several shapes for the sake of acoustic damping. One of them, quarter-wave resonator is illustrated in Fig. 3. The gas–liquid scheme injector has the same shape as quarter-wave resonator, but with different boundary condition at one end surface. That is, quarter-wave resonator has open end at the matching surface with the chamber and closed end at the other as shown in Fig. 3, whereas the present injector has open ends at both ends. Of course, the condition at the matching surface is the interior boundary condition and is not forced by numerical treatment. At only one end of injector inlet, the boundary condition is enforced numerically to be acoustically open boundary condition of $p' = 0$ ($Z = 0$).

In accordance with these boundary conditions at end surfaces, acoustic-pressure node and anti-node [28] are formed at one end and the other, respectively, in quarter-wave resonator. Therefore, it functions literally as

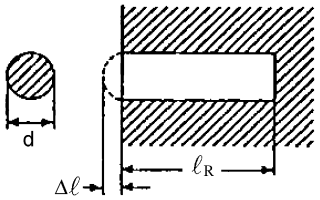

Fig. 3. Quarter-wave resonator [9].

quarter-wave resonator. In a similar manner, the present injector may function as half-wave resonator since acoustic pressure nodes are formed at both ends of the injector. Then, the mechanism of acoustic damping or absorption occurring in quarter-wave resonator [1,9,10] could be applied to the injector as well. The only difference between them is the wavelength; a quarter and a half of a full wavelength, respectively.

The tuning frequency of quarter-wave resonator is expressed by [9]

$$f_0 = \frac{c_R}{4(l_R + \Delta l)}, \tag{4}$$

where f_0 denotes tuning frequency, i.e., the frequency of harmful acoustic oscillation intended to be damped in the chamber, c_R sound speed of the fluid in the resonator, l_R the length of the resonator, and Δl length or mass correction factor. If the hypothesis aforementioned is valid, Eq. (4) can be still used even for injector design with the substitution of a numeral "2" for "4" of Eq. (4). And then, the tuning length of the injector for maximum acoustic damping can be derived as

$$l_{\text{inj}} = \frac{c_{\text{inj}}}{2f_0} - \Delta l, \tag{5}$$

where l_{inj} and c_{inj} denote the injector length and sound speed of the fluid in the injector, respectively. This equation expresses theoretically the optimum length of the injector canceling the acoustic oscillation coming from the chamber with the frequency of f_0. Out of numerous acoustic modes, the first tangential ($1T$) mode is intended to be damped by the injector in this study since it is known to be one of the most harmful modes in liquid rocket engines [1].

4. Results and discussions

First, acoustic behavior in unbaffled chamber with a single injector is investigated for cold condition over the wide range of injector length, l_{inj}. Next, baffled chamber with a single injector for both cold and hot conditions is analyzed to examine how baffle installation affects the acoustic damping mechanism of the injector and to calculate realistic injector length tuned for actual or hot condition in a quantitative manner. Then, acoustic characteristics in the chamber with numerous injectors are investigated. And finally, effect of blockage at injector inlet is examined.

4.1. Acoustic damping by a single injector

In the unbaffled chamber with a single injector, acoustic analyses are conducted with variable injector length, l_{inj} of 0 to 700 mm. Acoustic-pressure responses at the monitoring point are calculated as a function of the excitation frequency and are shown in Fig. 4 with the emphasis on the two lowest resonant modes of the chamber. As shown in this figure, two peak responses occur at 414 and 548 Hz in the chamber without injector, i.e., $l_{\text{inj}} = 0$. Judging from spatial distribution of acoustic pressure (acoustic field) at each mode, the first and second peaks have been identified as the first longitudinal ($1L$) and the first tangential ($1T$) modes, respectively. The acoustic resonant frequencies, f_{1L} and f_{1T}, are rarely affected by single-injector installation and its length, whereas acoustic amplitude of $1T$ mode is affected appreciably, which is shown more clearly in Fig. 5. This indicates that the injector can play a significant role in acoustic damping or absorption of the

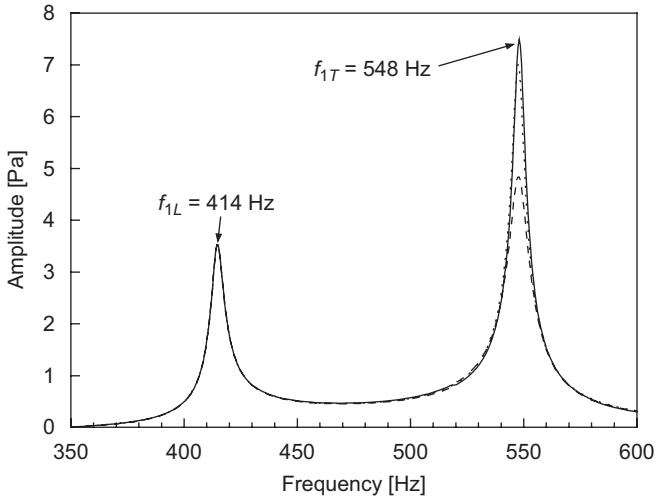

Fig. 4. Acoustic-pressure responses in unbaffled chamber with a single injector (solid line: $l_{\text{inj}} = 0$ mm, dotted line: $l_{\text{inj}} = 250$ mm, dashed line: $l_{\text{inj}} = 300$ mm).

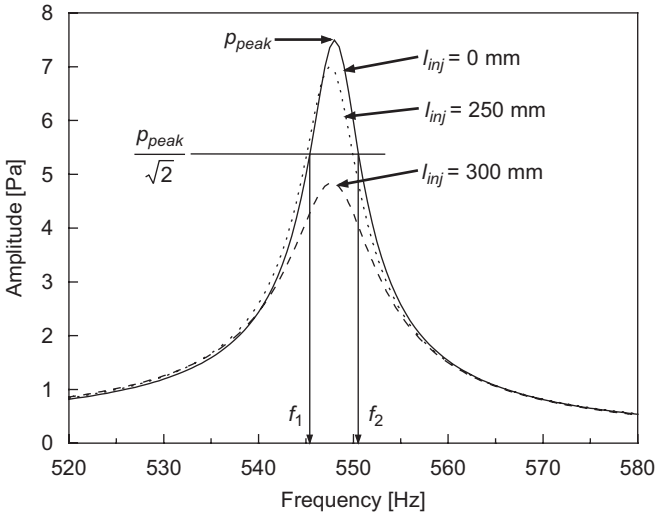

Fig. 5. Acoustic-pressure responses near f_{1T} for several injector lengths.

tuned-frequency oscillation ($1T$). To evaluate acoustic damping capacity of the injector quantitatively, a parameter of damping factor, η is introduced and evaluated by bandwidth method in the form [9,21],

$$\eta = \frac{f_2 - f_1}{f_{\text{peak}}}, \tag{6}$$

where f_{peak} is the frequency at which the peak response (p_{peak}) appears and f_1 and f_2 are the frequencies at which the pressure amplitude corresponds to $p_{\text{peak}}/\sqrt{2}$ with $f_2 > f_1$. This equation indicates that the damping factor becomes higher as the bandwidth is broadened as demonstrated in Fig. 5.

Based on the acoustic-response data calculated with variable injector length, damping factors are calculated by Eq. (6) as a function of l_{inj} and are shown in Fig. 6. As l_{inj} increases from 0, damping factor increases gradually and then, does rapidly near $l_{\text{inj}} = 300$ mm. As l_{inj} increases further, damping factor decreases rapidly and then, the similar cyclic pattern is repeated. Two peaks of η occur at $l_{\text{inj}} = 303$ and 610 mm.

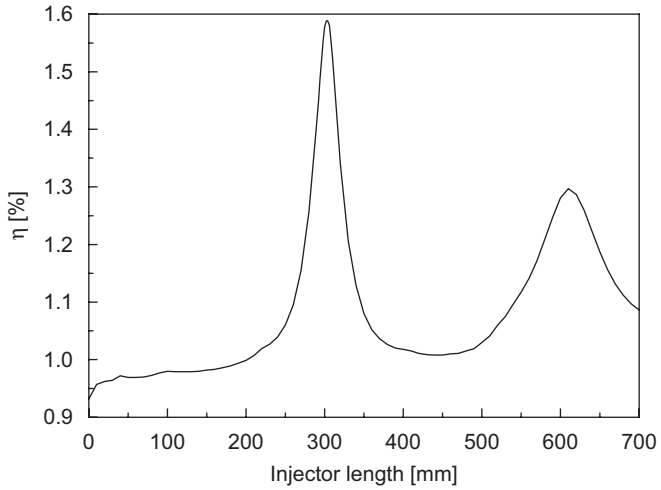

Fig. 6. Damping factors as a function of injector length at $1T$ mode.

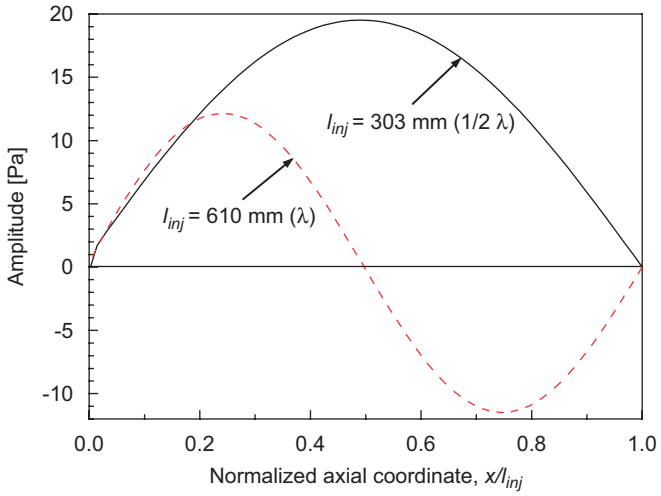

Fig. 7. Longitudinal profiles of pressure-fluctuation amplitudes (real parts) inside injectors with $l_{\text{inj}} = 303$ and 610 mm.

With $f_{1T} = 548$ Hz, the wavelength of the 1st longitudinal overtone mode inside the injector is calculated to be 620 mm. Accordingly, the injector length of 303 mm, at which the largest peak occurs, corresponds to a half-wavelength of $1L$ overtone mode oscillating in the injector with the same frequency as that of $1T$ mode in the chamber. The exact length of a half-wavelength, $(1/2)\lambda$ is calculated to be 310 mm and the error of 7 mm can be attributed to the length correction, Δl as indicated in Eq. (5). From Fig. 6, the second largest peak occurs at $l_{\text{inj}} = 610$ mm, which corresponds to λ. Although not shown here, the subsequent peaks have been observed in order at $l_{\text{inj}} = (3/2)\lambda$, 2λ, and $(5/2)\lambda$, etc. All of these lengths satisfy open condition at both ends of the injector and thus, integer multiples of $(1/2)\lambda$ correspond to tuning length of injector for efficient acoustic damping. Out of them, the optimum tuning length is a half-wavelength at which maximum damping occurs as shown in Fig. 6. To examine this point, longitudinal profiles of pressure fluctuation inside injectors with two lengths of $l_{\text{inj}} = (1/2)\lambda$ and λ are shown in Fig. 7. Pressure-fluctuation amplitude at $l_{\text{inj}} = (1/2)\lambda$ is much higher than at $l_{\text{inj}} = \lambda$. Higher fluctuation inside injector indicates more cancellation of pressure wave flowing into the injector from the chamber. Accordingly, the half-wave injector is more effective in damping out pressure oscillation than the injectors with the other lengths.

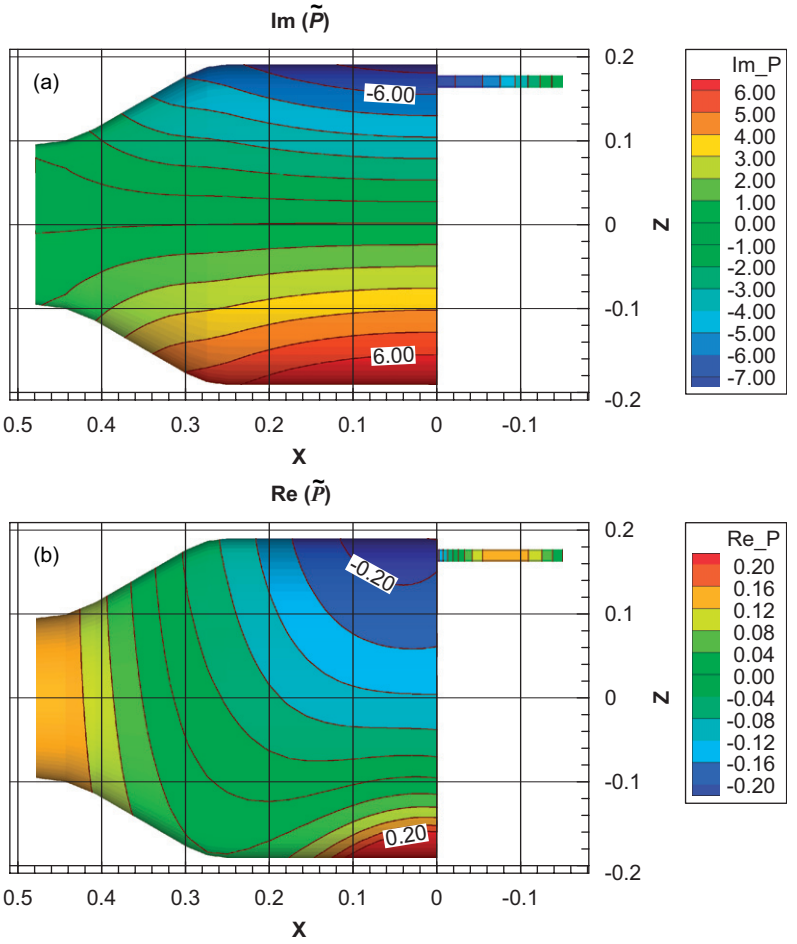

Fig. 8. Acoustic fields of $1T$ mode resonant at 548 Hz in unbaffled chamber with $l_{inj} = (1/4)\ \lambda$.

On the other hand, when reasoned in an opposite or contrary manner, the mal-tuning of the injector will be observed at $l_{inj} = (1/4)\lambda$, $(3/4)\lambda$, and $(5/4)\lambda$, etc., which is verified by the result in Fig. 6. Acoustic-pressure fields in the chambers with mal-tuned and optimally tuned injectors are demonstrated in Figs. 8 and 9, respectively. From imaginary parts of $\tilde{P}$, resonance of $1T$ mode is clearly formed in the chambers in both cases, but acoustic amplitude in the chamber with the injector of $l_{inj} = (1/2)\lambda$ is much smaller than that of $l_{inj} = (1/4)\lambda$. From real parts of $\tilde{P}$, it is found that half-wave injector responds sensitively to acoustic oscillation inflowing from the chamber, whereas quarter-wave injector acts independently of in-chamber oscillation. In the latter case, the injector has little contribution to acoustic damping since it does not respond to acoustic field in the chamber at all.

4.2. *Effect of baffle installation on acoustic tuning of injector*

In the preceding section, it has been found that the injector can be regarded as half-wave resonator from the viewpoint of acoustic damping. To enhance the reliability of combustion stabilization, baffled chamber would be adopted, where baffle hub and blades are mounted to the injector faceplate as shown in Fig. 10 [1,9,16]. Baffle is an obstacle placed in a chamber and it prevents transverse waves from being formed and weakens acoustic resonance of the transverse modes. Baffle installation affects acoustic field in the chamber in various aspects. Out of them, two effects are worth noting; one is that baffle makes acoustic waves of transverse (tangential and radial) modes longitudinalized within baffle compartments and the other is that the resonant

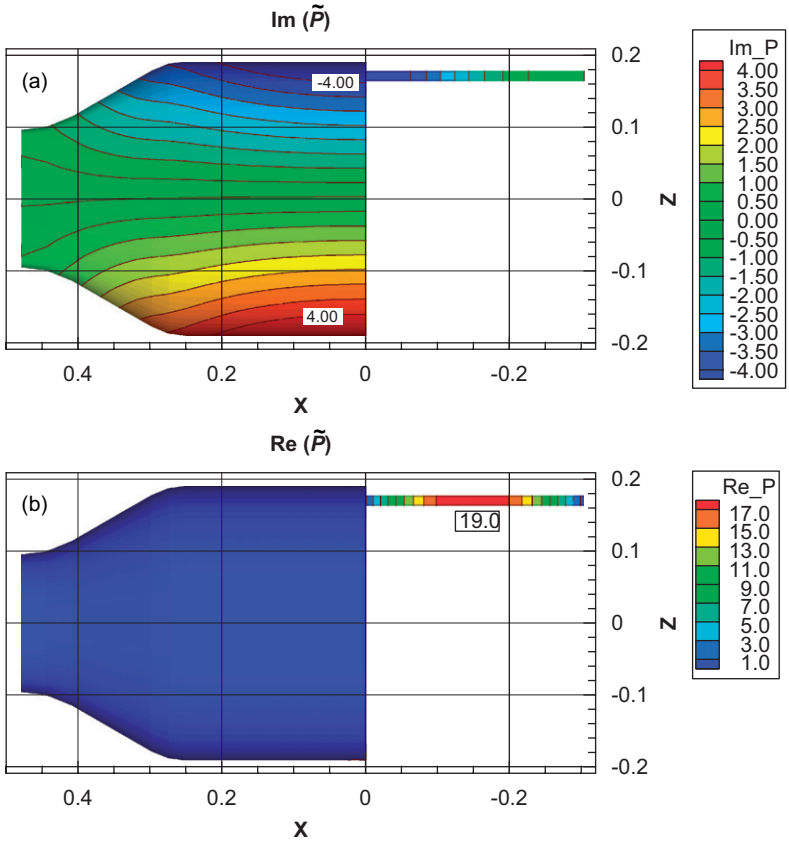

Fig. 9. Acoustic fields of $1T$ mode resonant at 548 Hz in unbaffled chamber with $l_{inj} = (1/2)\ \lambda$.

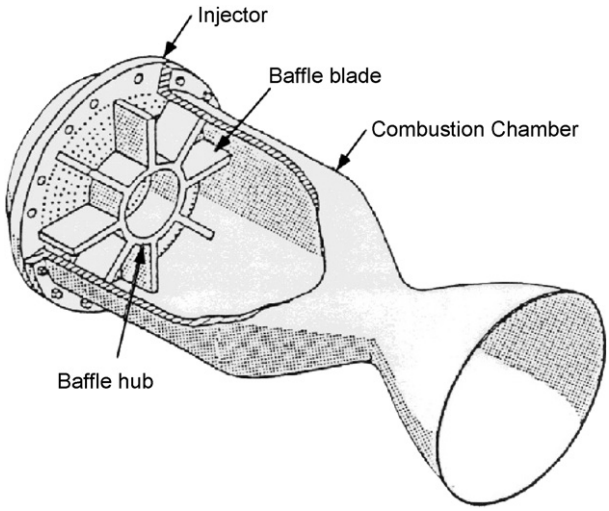

Fig. 10. Baffled combustion chamber with one hub and six blades [1].

frequencies of transverse modes shift to lower ones [9]. The former effect may prevent the injector from acting as a half-wave resonator since the interior boundary condition of pressure node may be violated for smooth matching with the longitudinalized wave near the faceplate. This hypothesis is demonstrated in Fig. 11. If this is true, the injector might be act as the quarter-wave resonator, but it is distinct from one shown in Fig. 3.

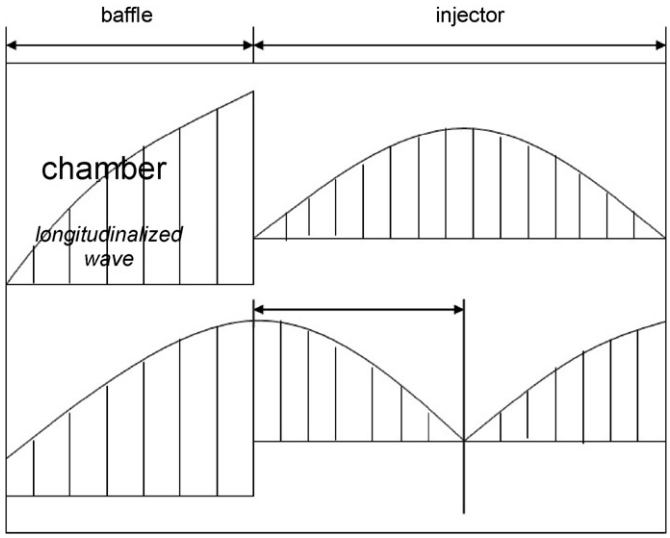

Fig. 11. Hypothetical diagram of pressure oscillation caused by baffle-injector coupling.

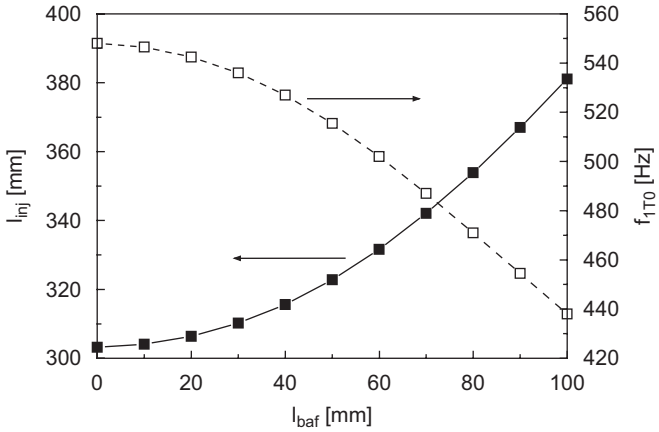

Fig. 12. Optimum injector lengths as a function of baffle length for cold condition in baffled chamber.

On the other hand, the latter effect can cause the tuning length elongated depending on the frequency shift. This point is predictable from Eq. (5).

To examine these two points, calculations of acoustic responses have been repeated in baffled chamber with variable baffle length, l_{baf}. Here, the baffle consists of one hub and six blades. The numerical results show that the injector still acts as half-wave resonator even in baffled chamber. But, the optimum injector length depends on baffle length and is shown as a function of l_{baf} in Fig. 12. As predicted, f_{1T0} decreases with baffle length. The lengths are the almost same as ones calculated from Eq. (5) with f_{1T0} substituted for f_0 at each baffle length. Accordingly, the tuning length of the injector is still a half-wavelength of acoustic oscillation, irrespective of baffle installation and the hypothesis aforementioned is not practically applicable to acoustic tuning of the injector. This fact indicates further that the injector tuning does not depend on the acoustic mode shape, but only on the acoustic frequency in the chamber.

As shown in Fig. 12, optimum tuning lengths are unrealistically long, which results from calculation for cold condition. To realize the length quantitatively, sample calculation is conducted for exemplary hot condition of $c_0 = 1270\,\mathrm{m/s}$, $\rho_0 = 13.1\,\mathrm{kg/m^3}$, $c_{inj} = 475.4\,\mathrm{m/s}$, and $\rho_{inj} = 103.3\,\mathrm{kg/m^3}$ [30]. Optimum injector lengths are shown as a function of baffle length in Fig. 13. Compared with results in Fig. 12, the higher resonant

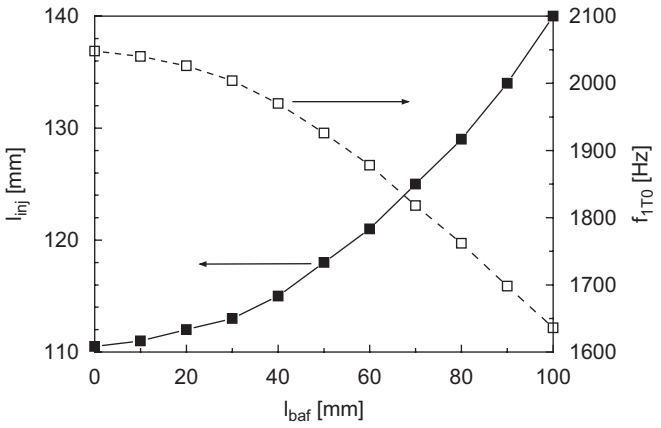

Fig. 13. Optimum injector lengths as a function of baffle length for hot condition in baffled chamber.

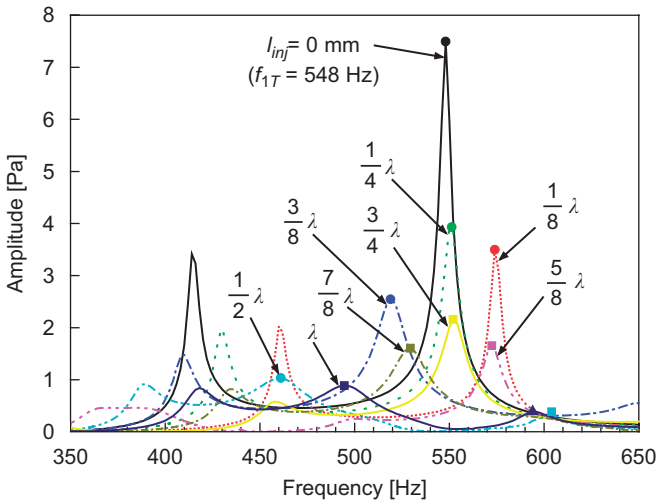

Fig. 14. Acoustic-pressure responses in unbaffled chamber with numerous injectors (symbols of ●, ■, and ▲ indicate peaks of $1T$, $1T1L^*$, and $1T2L^*$ modes, respectively).

frequencies result from high sound speed, i.e., high temperature in the actual combustion chamber and thereby, optimum injector lengths have reasonable values near about 100 mm.

4.3. Peculiar acoustic coupling induced by multi-injectors

Since actual engines usually have hundreds of injectors on their faceplate, effects of the numerous injectors are investigated in unbaffled chamber with 61 identical injectors, of which diameter is 30 mm. The injectors are distributed uniformly on the faceplate. By mounting these numerous injectors, the injectors occupy 38% of faceplate in area. That is, the ratio of open area to faceplate area, σ_A amounts to 0.38.

Acoustic-pressure responses at the monitoring point are calculated as a function of the excitation frequency with the variable, l_{inj} and are shown in Fig. 14. The injector length ranges from 0 to λ. As shown in this figure, both acoustic frequency and amplitude are varied appreciably depending on the length of the injectors. These characteristics are quite different from ones with a single injector in Figs. 4 and 5. Acoustic response at $l_{inj} = 303$ mm, i.e., $(1/2)\lambda$, has three peaks at frequencies of 390, 460, and 604 Hz, of which amplitudes are appreciably small compared with ones at $l_{inj} = 0$ mm. These acoustic responses indicate sufficient damping or

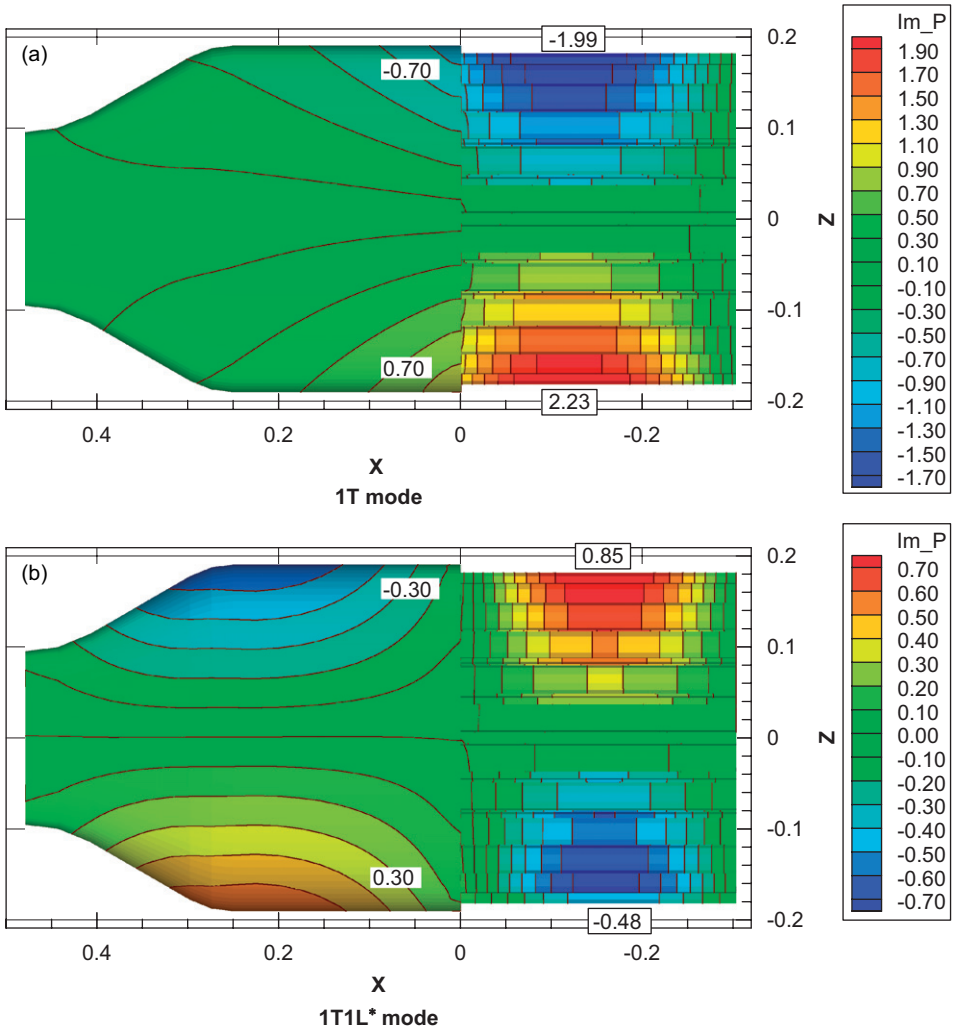

Fig. 15. Acoustic fields in unbaffled chamber with numerous injectors of $l_{inj} = (1/2)\ \lambda$; (a) $1T$ mode resonant at 460 Hz and (b) $1T1L^*$ mode resonant at 604 Hz.

absorption of acoustic waves and especially, complete damping-out of acoustic wave oscillating at $f = 548$ Hz. From examination of acoustic fields formed at each peak, they are identified as $1L$, $1T$, and $1T$-like modes in order of ascending frequency. The third peak with 604 Hz shows up newly here and it has not been observed in the chamber with a single injector. The acoustic fields at 460 and 604 Hz are shown in Fig. 15. Fig. 15a shows acoustic field of $1T$ mode, but it is nearly damped out and sustains just weak resonance of $1T$ mode. On the other hand, in Fig. 15b, the acoustic field at 604 Hz shows quite peculiar behavior with the same injector length of $(1/2)\lambda$. If we observe the field only in the chamber excluding the injector part, it is close to half-pattern of $1T1L$ mode, i.e., the combined mode of $1T$ and $1L$, rather than to pure $1T$ mode. From the acoustic field in full domain including both chamber and injectors, the point is more clarified since spatial distribution of acoustic wave has that of $1T1L$ exactly. But, this mode is distinct from genuine $1T1L$ mode formed only in the chamber and here, it is denoted by $1T1L^*$; injector-coupled $1T1L$ mode.

Considering the acoustic fields shown in Fig. 15b, we can find out that the novel mode results from acoustic coupling between chamber and injectors. In the chamber with a single injector, where σ_A amounted to only 0.14%, the peculiar acoustic coupling has hardly been observed as shown in Figs. 4, 5, 8 and 9. Through further calculations not shown here, it has been found that the coupling shows up more evidently as the area

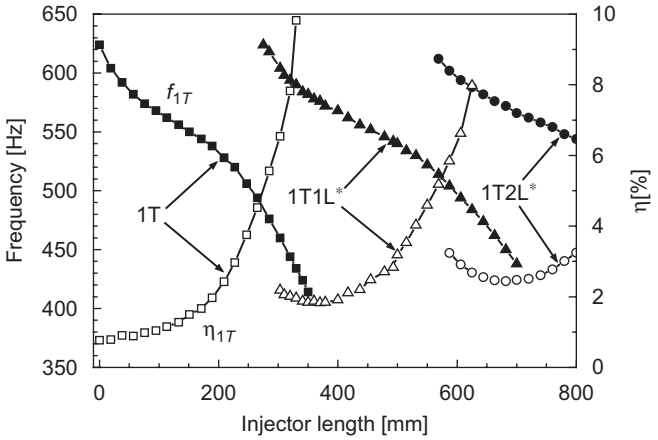

Fig. 16. Acoustic frequencies and damping factors of pure and injector-coupled $1T$ modes as a function of injector length in unbaffled chamber with numerous injectors (solid symbols: frequency, void symbols: damping factor).

ratio, σ_A increases. This is that the one end of injectors on the matching surface with the chamber tends to act as the interior volume rather than the interior boundary as σ_A increases. Accordingly, pressure node is not formed clearly any more at the end. At the upper limit of unity σ_A, i.e., $\sigma_A = 1$, distinction or boundary between chamber and injectors disappears and they will make a single volume.

Next, effects of the acoustic coupling on injector tuning are investigated. For this, acoustic resonant frequencies of $1T$-family modes and their damping factors are calculated as a function of l_{inj} and are shown in Fig. 16. As l_{inj} increases, acoustic frequency decreases gradually over the wide range of injector length beyond $l_{\text{inj}} = (1/2)\lambda$. On the other hand, damping factor increases gradually and then, does rapidly. The acoustic field in the chamber with infinitely short injectors is shown in Fig. 17. With non-zero injector length, the faceplate becomes partial wall-boundary surface with numerous holes. Accordingly, locally open condition affects the acoustic field. Due to the modified boundary condition on the faceplate, $1T$ mode is longitudinalized locally near the faceplate.

An interesting behavior is observed at $l_{\text{inj}} = (1/4)\lambda$, which corresponds to the worst or mal-tuned length in the chamber with a single injector as mentioned in the preceding section. From Figs. 14 and 16, the acoustic frequency at the length of $(1/4)\lambda$ coincides with that at $l_{\text{inj}} = 0$, i.e, original frequency. This point verifies mal-tuning of $(1/4)\lambda$-injector as well. That is, the injectors of $l_{\text{inj}} = (1/4)\lambda$ are acoustically decoupled with the chamber even in case of numerous injectors. But, the damping factor is larger than original damping factor by 55%, which contradicts the result of Fig. 6. From this point, it is found out that the increase in damping factor by numerous injectors arises purely from boundary absorption at injector walls, not wave cancellation inside the injectors. Due to numerous injectors, the boundary absorption contributes far more to increase in damping factor than with a single injector.

As l_{inj} approaches a half-wavelength of 303 mm, f_{1T} decreases moderately and η_{1T} increases rapidly. The $1T$ mode becomes weaker and weaker, and finally, it is completely damped out. The mode is not observed any longer with the injector length over 350 mm. In the meantime, new mode of $1T1L^*$ starts to show up with higher frequency just before $l_{\text{inj}} = (1/2)\lambda$. From exhaustive calculations, it starts from $l_{\text{inj}} = 275$ mm, at which f_{1T1L^*} is 624 Hz. And its damping factor has much smaller values than that of $1T$ mode in the overlapping region with $1T$ mode. Accordingly, it is found that the new coupled-mode degrades appreciably the damping effect of the tuned injectors.

The frequency of $1T1L^*$ mode is evaluated approximately from the acoustic field, e.g., one shown in Fig. 15b, as follows. The acoustic frequency of $1T1L$ combined mode is expressed as [19,27]

$$f_{1T1L} = \sqrt{f_{1T}^2 + f_{1L}^2}. \tag{7}$$

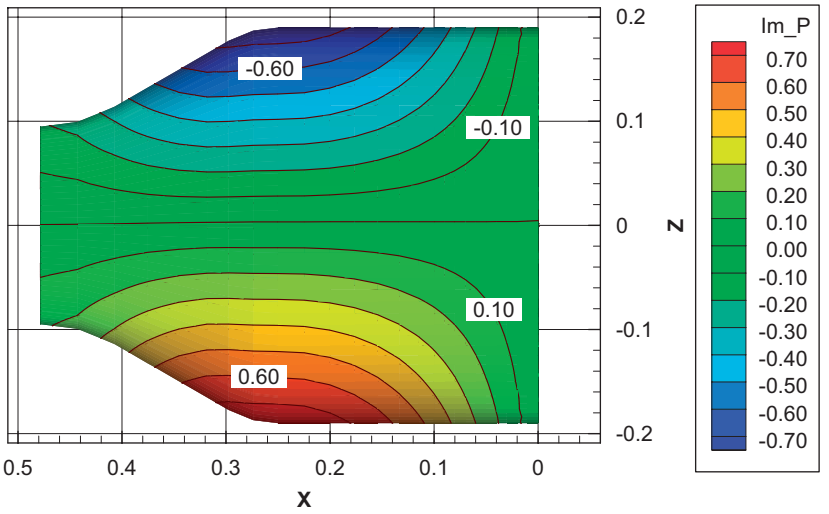

Fig. 17. Acoustic fields of $1T$ mode at 624 Hz in unbaffled chamber with numerous injectors of $l_{inj} = 10^{-7}$ mm.

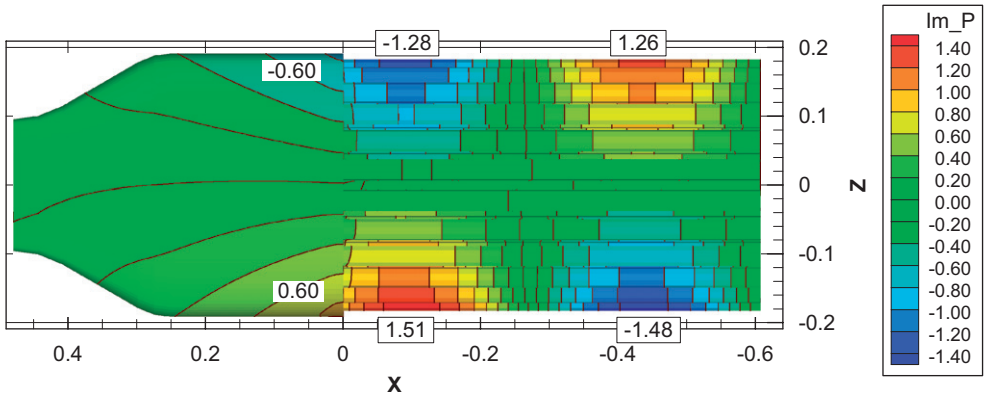

Fig. 18. Acoustic fields of $1T1L^*$ mode at 494 Hz in unbaffled chamber with numerous injectors of $l_{inj} = \lambda$.

In the preceding section, f_{1T} and f_{1L} are calculated 548 and 414 Hz, respectively. From Fig. 15b, it is found that only the first half-part of the injector is involved in constituting acoustic field of $1T1L^*$ mode since pressure anti-node is formed about the center of the injector. Then, virtually, the frequency of the injector-coupled $1L$ mode, $f_{1L}{}^*$ can be calculated as

$$f_{1L}^* = f_{1L}\frac{L_{\text{eff}}}{L_{\text{eff}} + L_{\text{inj}}^*}, \tag{8}$$

where L_{eff} denotes effective chamber length, calculated approximately by $L_e + (2/3)(L_{\text{th}}–L_e)$ [27], and L_{inj}^* the length of the injector involved in coupled $1L$ mode. Near $l_{\text{inj}} = (1/2)\lambda$, L_{inj}^* corresponds to a half or so of the actual injector length. Using Eqs. (7) and (8), we calculated $f_{1L}^* = 308$ Hz and thereby, $f_{1T1L^*} = 629$ Hz. The value of f_{1T1L^*} calculated by the analytic equations, is in a good agreement with one from the numerical analysis; 629 vs. 624 Hz. This agreement also verifies quantitatively that the new mode can be regarded as the injector-coupled $1T1L$ mode.

As l_{inj} increases further, f_{1T1L^*} decreases gradually and η_{1T1L^*} increases. These behaviors are the same as in case of $1T$ mode. As l_{inj} approaches a full wavelength, the $1T1L^*$ mode becomes weaker and weaker, and

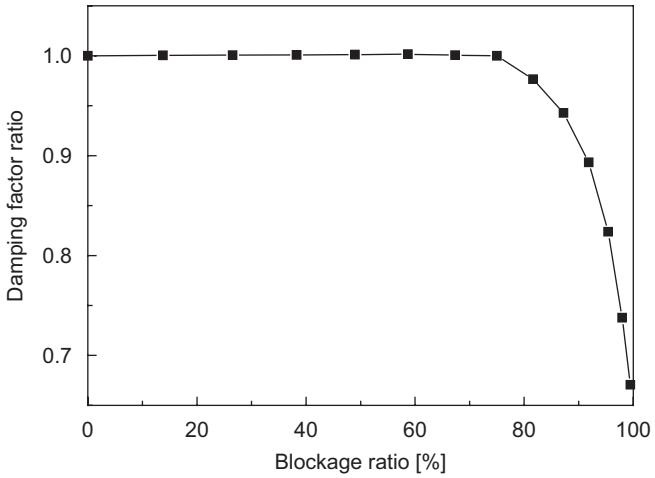

Fig. 19. Damping factor ratio as a function of blockage ratio in unbaffled chamber with a single injector of $l_{inj} = (1/2)\ \lambda$.

finally, it is completely damped out. Over the range of l_{inj} beyond 475 mm, f_{1T1L^*} decreases below the original frequency of $1T$ mode, $f_{1T} = 548$ Hz as shown in Fig. 16. This behavior seems to be impossible judging from Eq. (7). For example, Fig. 18 shows acoustic field with $l_{inj} = 606$ mm at 494 Hz, which is much less than 548 Hz. As shown in this figure, the left half-part of $1T1L^*$ penetrates into the injector, and thereby, the analytical equations from theoretical acoustics is not valid any longer. However, the acoustic field still shows $1T1L^*$ mode. In a similar manner to the case of $1T$ mode, the mode is not observed any longer with the injector length over 700 mm and in the meantime, the additional new mode of $1T2L^*$ starts to show up near $l_{inj} = \lambda$. Accordingly, overall behaviors of acoustic frequencies and damping factors have cyclic but discontinuous patterns as shown in Fig. 16. The acoustic modes of $1T$, $1T1L^*$, $1T2L^*$, and so on, show up sequentially, but with the overlapping region with the neighboring mode. The higher modes as from $1T1L^*$ arise from acoustic coupling between chamber and injectors, which indicates that acoustics inside the injector interacts with ones in the chamber and the injector is no longer original passive device.

As aforementioned, the tuning length of the injector corresponds to a half-wavelength of $1T$ mode. But, with peculiar acoustic coupling considered, it should be modified since the new coupling mode shows up near the original tuning length, leading to small damping factor. Accordingly, when the tuning length is selected, two points should be satisfied; one is to bring out as high damping factor as possible and the other is to avoid injector-coupled modes. Then, from Fig. 16, it can be found that the best tuning length should be selected a bit less than a half-wavelength.

4.4. Effect of blockage at injector inlet

Another design parameter for acoustic tuning is the orifice diameter at gas–propellant (GO_x) inlet, d_{in} as shown in Fig. 1. For similarity, it is normalized by the inner diameter of the injector, d_{inj} and thereby, the normalized parameter of blockage ratio is introduced in the form

$$B = \frac{d_{inj}^2 - d_{in}^2}{d_{inj}^2}, \tag{9}$$

which denotes the ratio of the blocked area to the injector cross-sectional area.

Acoustic-pressure responses are calculated over the wide range of B in the chamber with a single injector of $l_{inj} = (1/2)\lambda$. From the numerical data, damping factor ratio defined as $\eta_B/\eta_{B=0\%}$, is calculated and shown in Fig. 19. Damping factor maintains a near-constant value with blockage ratio and then, decreases rapidly at high blockage ratio over 75%. This indicates that the injector tuned optimally at wide-open

inlet, i.e., $B = 0\%$, does not play a role as half-wave resonator at higher blockage ratio due to change of boundary condition. But, it is worthy of note that damping capacity is maintained over the broad range of B up to 75%.

5. Conclusion

Acoustic-pressure responses in the chamber with gas–liquid scheme injector have been investigated numerically by adopting linear acoustic analysis. This analysis is intended to check the possibility of acoustic damping through proper injector design and the role of the injector as acoustic resonator or absorber is studied extensively in the chambers with a single injector and multi-injectors. The first tangential mode has been selected as a target mode to be damped or absorbed in this study.

Acoustic behaviors in the chamber with a single injector have shown that the injector can absorb acoustic oscillation in the chamber most effectively when it has the tuning length of a half-wavelength with respect to the acoustic frequency to be damped. In other words, it acts effectively as half-wave resonator; the optimum length for acoustic tuning should be a half-wavelength in order to maximize acoustic absorption. This study shows also that the high blockage at injector inlet can degrade acoustic damping.

Effects of the injector on acoustic absorption have been found to be critical and significant. Accordingly, it is proposed that the effects should be considered elaborately in injector design for fine-tuning. Although, baffle installation modifies the acoustic field locally near the injector faceplate, the injector tuning length of $(1/2)\lambda$ is not affected by it. When numerous injectors are mounted to the chamber, open area on the faceplate will not be negligibly small any longer. As open-area ratio increases, peculiar characteristics, i.e., acoustic coupling between the chamber and injectors show up. Acoustics inside injectors interacts with in-chamber acoustic field, and thereby, the injectors behave acoustically on a level with the chamber. As a result of acoustic coupling, new acoustic modes show up near the injector lengths of $(1/2)\lambda$, λ, and $(3/2)\lambda$, etc. They have been identified as the injector-coupled modes of $1T1L$, $1T2L$, and higher formed in the full domain including injector part. And thereby, acoustic-damping capacity of the tuned injector can be appreciably degraded. With the coupling considered, the tuning length should be modified to be a bit less than a half-wavelength to avoid the injector-coupled modes. Besides, it is shown that actual injector length can be obtained quantitatively from the present acoustic analyses for hot condition simulating high temperature in the combustion chamber.

Although the first tangential mode is concentrated on in this study, the present findings are not limited to the specific acoustic mode, but applicable to any acoustic modes. Based on the present results, it is proposed that injector should be designed for propellants injection and at the same time, for acoustic damping. When it is tuned finely or properly, acoustic stability can be improved considerably and further, it makes the classical combustion-stabilization devices such as baffle and resonators unnecessary. Attention here has been focused on linear acoustics. To describe acoustic function of the injector more completely, it is recommended that nonlinear behaviors of acoustic field need to be investigated. It will be the subject of future work.

Acknowledgments

This work was supported by the Korea Research Foundation Grant (KRF-2004-002-D00059).

References

[1] D.J. Harrje, F.H. Reardon (Ed.), *Liquid Propellant Rocket Combustion Instability*, SP-194, 1972, NASA.
[2] J.W.S. Rayleigh, *The Theory of Sound*, Vol. 2, Dover, New York, 1945, pp. 226–235.
[3] K.R. McManus, T. Poinsot, S.M. Candel, A review of active control of combustion instabilities, *Progress in Energy and Combustion Science* 19 (1993) 1–29.
[4] F.E.C. Culick, V. Yang, Overview of combustion instabilities in liquid-propellant rocket engines, in: V. Yang, W.E. Anderson (Eds.), *Liquid Rocket Engine Combustion Instability*, Vol. 169, Progress in Astronautics and Aeronautics, AIAA, Washington, DC, 1995, pp. 3–37.
[5] J.C. Oefelein, V. Yang, Comprehensive review of liquid-propellant combustion instabilities in F-1 engines, *Journal of Propulsion and Power* 9 (1993) 657–677.

[6] S. Ducruix, T. Schuller, D. Durox, S.M. Candel, Combustion dynamics and instabilities: elementary coupling and driving mechanisms, *Journal of Propulsion and Power* 19 (2003) 722–734.
[7] C.-C. Hantschk, D. Vortmeyer, Numerical simulation of self-excited thermoacoustic instabilities in a Rijke tube, *Journal of Sound and Vibration* 217 (1999) 511–522.
[8] S. Dawson, J.A. Fitzpatrick, Measurement and analysis of thermoacoustic oscillations in a simple dump combustor, *Journal of Sound and Vibration* 230 (2000) 649–660.
[9] E. Laudien, R. Pongratz, R. Pierro, D. Preclik, Experimental procedures aiding the design of acoustic cavities, in: V. Yang, W.E. Anderson (Eds.), *Liquid Rocket Engine Combustion Instability*, Vol. 169, Progress in Astronautics and Aeronautics, AIAA, Washington, DC, 1995, pp. 377–399.
[10] R.B. Keller Jr. (Ed.), *Liquid Rocket Engine Combustion Stabilization Devices*, SP-8113, 1974, NASA.
[11] J.S. Kim, F.A. Williams, Effect of non-homogeneities on the eigenmodes of acoustic pressure in combustion chambers, *Journal of Sound and Vibration* 209 (1998) 821–843.
[12] T. Conrad, A. Bibik, D. Shcherbik, E. Lubarsky, B.T. Zinn, Control of instabilities in liquid fueled combustor by modification of the reaction zone using smart fuel injector, AIAA Paper 2004-4029, July 2004.
[13] M. Mettenleiter, E. Haile, S.M. Candel, Adaptive control of aeroacoustic instabilities, *Journal of Sound and Vibration* 230 (2000) 761–789.
[14] C.L. Oberg, Combustion stabilization with acoustic cavities, *Journal of Spacecraft and Rockets* 8 (1971) 1220–1225.
[15] T.L. Acker, C.E. Mitchell, Combustion zone-acoustic cavity interactions in rocket combustors, *Journal of Propulsion and Power* 10 (1994) 235–243.
[16] J.M. Wicker, M.W. Yoon, V. Yang, Linear and non-linear pressure oscillations in baffled combustion chambers, *Journal of Sound and Vibration* 184 (1995) 141–171.
[17] D.K. Huzel, D.H. Huang, *Modern Engineering for Design of Liquid-Propellant Rocket*, Vol. 147, Progress in Astronautics and Aeronautics, AIAA, Washington, DC, 1992 (35pp).
[18] G.P. Sutton, History of liquid-propellant rocket engines in Russia, formerly the Soviet Union, *Journal of Propulsion and Power* 19 (2003) 1008–1037.
[19] M.J. Zucrow, J.D. Hoffman, *Gas Dynamics*, Vol. II, Wiley, New York, 1977 (Chapter 15).
[20] T. Tsuji, T. Tsuchiya, Y. Kagawa, Finite element and boundary element modelling for the acoustic wave transmission in mean flow medium, *Journal of Sound and Vibration* 255 (2002) 849–866.
[21] S.-K. Kim, H.J. Kim, W.S. Seol, C.H. Sohn, Acoustic stability analysis of liquid propellant rocket combustion chambers, AIAA Paper 2004-4142, July 2004.
[22] S.C. Chapra, R.P. Canale, *Numerical Methods for Engineers*, second ed., McGraw-Hill, Singapore, 1989 (Chapter 25).
[23] Y. Saad, SPARSKIT: A Basic Tool Kit for Sparse Matrix Computations, Ver. 2, Technical Report 90-20, Research Institute for Advanced Computer Science, NASA Ames Research Center, Moffet Field, CA, 1990.
[24] S.-K. Kim, H.J. Kim, C.H. Sohn, Development of analysis code for evaluation of acoustic stability of rocket engine combustor with various designs, *Journal of the Korean Society for Aeronautical and Space Sciences* 32 (2004) 110–116.
[25] M.S. Natanzon, *Combustion Instability*, Mashinostroyeniye, Moscow, Russian Federation, 1986 (Chapter 3).
[26] C.H. Sohn, H.C. Cho, Numerical analysis of acoustic characteristics in gas turbine combustor with spatial non-homogeneity, *KSME International Journal* 18 (2004) 1461–1469.
[27] A.F. Agarkov, A.A. Narizny, A.K. Nedashkovsky, V.P. Pikalov, A.A. Shibanov, Acquisition, Processing, and Delivery of Data on Characteristics of Stable Combustion as Applied to Bipropellant Impinging—Jets Injectors, Research Institute of Chemical Machine Building (NIICHIMMASH), Rept. No. 1/512-2000-07, Moscow, Russian Federation, 2000.
[28] L.E. Kinsler, A.R. Frey, A.B. Coppens, J.V. Sanders, *Fundamentals of Acoustics*, fourth ed., Wiley, New York, 2000 (Chapter 2).
[29] C.H. Sohn, Y.-M. Kim, A numerical study on acoustic behavior in combustion chamber with acoustic cavity, *Journal of the Korean Society for Aeronautical and Space Sciences* 30 (2002) 28–37.
[30] A.K. Nedashkovsky, A.A. Narizny, V.P. Pikalov, A.A. Shibanov, Studies of Acoustic Behavior of Model Combustion Chambers and Combustion Stability Characteristics of Different Injection Elements under Model Operating Conditions, Research Institute of Chemical Machine Building (NIICHIMMASH), Rept. No. 512-2002-03, Moscow, Russian Federation, 2002.